Toward a Laser-Driven Traveling-Wave Linac on a Chip

Weihao Liu,[1,*] Liwen Zhang,[2] Yucheng Liu,[1] Qika Jia,[2] Baogen Sun,[2] and Hongliang Xu[2]

[1] *College of Electronic and Information Engineering, Nanjing University of Aeronautics and Astronautics, Nanjing, Jiangsu 211106, China*

[2] *National Synchrotron Radiation Laboratory, University of Science and Technology of China, Hefei, Anhui 230029, China*

(Received 13 June 2022; revised 2 March 2023; accepted 30 March 2023; published 21 April 2023)

Restricted by pulse dispersion, dephasing, and bunch deflection, it has been a challenging task to realize high-gain particle acceleration and bunch focusing by using an ultrashort-pulse laser to drive an integrable acceleration structure, which is necessary to develop an on-chip particle accelerator for practical applications. Here we propose a laser-driven traveling-wave linac (linear accelerator), which uses the cascade reflection and refraction of an ultrashort laser pulse on a microscale dielectric structure to achieve long-range laser-particle interaction, avoiding waveguide dispersion, and enhancing sustainable acceleration gradient. It is scalable and extensible, and can realize full-course particle acceleration by using a single laser source via the inverse Cherenkov effect. With this accelerator scheme, we further propose a dynamic synchronization and focusing method, which not only counteracts dephasing but also restrains the bunch spread and deflection caused by space-charge and emittance effects, realizing stable bunch transport and acceleration in a tiny-size bunch channel without resorting to the need for external focusing equipment. This accelerator scheme paves the way toward a high-efficiency laser-driven all-dielectric on-chip particle accelerator for practical applications.

DOI: 10.1103/PhysRevApplied.19.044066

I. INTRODUCTION

The concept of an on-chip particle accelerator using high-power ultrashort-pulse laser beams to drive microscale dielectric structures has attracted great interest in recent years [1–7]. In the available dielectric-laser-accelerator schemes based on the inverse Smith-Purcell effect [8–11], each laser pulse can be used only once for particle acceleration, so that the acceleration efficiency, the laser-particle interaction length, and the energy gain are greatly restricted. Utilizing a single laser import to realize long-range acceleration with high energy gain is a critical issue for the development of a practical laser-driven dielectric accelerator. Employing the traveling wave excited by a laser pulse to accelerate particles in a dielectric optical waveguide, similarly to a conventional rf traveling-wave linac (linear accelerator), is a promising and necessary solution to settle this issue. Great efforts have been made to this end, and laser-driven accelerators with various dielectric waveguides have been investigated [12–15]. Unfortunately, these available schemes encounter a series of challenges.

Firstly, the guided modes in conventional optical waveguides generally have serious waveguide dispersion, so that a short laser pulse, which possesses a broad spectral bandwidth, will be deformed as it propagates. To counteract pulse dispersion, a long-duration laser pulse with narrow spectral bandwidth has to be adopted, which restricts the sustainable acceleration gradient of the dielectric structure [16]. Secondly, when using a high-power-density laser pulse to accelerate subrelativistic particles, the dephasing (phase slippage) will be remarkable, which restricts the synchronization length between particles and the guided wave. To increase the synchronization length, complicated waveguiding and laser-power delivery systems have to be applied [17–19]. Thirdly, the transverse electromagnetic fields in an optical waveguide will cause particle deflection, and the space-charge effect, together with the beam emittance, will lead to bunch spread. Both the deflection and spread of particles will decrease the pass ratio, reducing the accelerated bunch charge. To simultaneously obtain nondispersive propagation of laser pulses along accelerating structures, stable bunch transport in a tiny-size bunch channel, and continuous synchronization of subrelativistic particles with laser-driven fields has been a long-term challenge in the development of a high-efficiency and high-energy-gain on-chip laser-driven traveling-wave particle accelerator.

In the present paper, we propose a novel laser-driven traveling-wave linac. It employs the cascade reflection

*liuwhao@nuaa.edu.cn

and refraction of ultrashort laser pulses from multistage microscale dielectric prisms on a chip to generate, in effect, a longitudinal traveling wave, which can be synchronized with the electron bunch at each stage, realizing cascade bunch acceleration. By this means, it effectively avoids waveguide dispersion and enhances the sustainable acceleration gradient. In each stage, the bunch acceleration is realized via the inverse Cherenkov effect [20–23], which uses the fundamental evanescent waves induced by the total internal reflection of light at a planar dielectric surface to accelerate particles [24–26].

With this accelerator scheme, we further propose a dynamic synchronization and focusing method, which can not only counteract dephasing but also realize bunch focusing by using the transverse fields excited by the drive laser. The focusing strength can be adjusted by tuning the dynamic synchronization phase and by changing the laser field intensity, so that stable bunch transport can be acquired in a tiny-size bunch channel without resorting to external focusing equipment, which is crucial for the miniaturization of particle accelerators. Hence, the proposed scheme promises a scalable and extensible accelerator which can realize full-course particle acceleration and bunch manipulation by using a single pair of laser pulses; this paves the way toward a high-efficiency on-chip traveling-wave linac for practical applications.

II. MODEL DESCRIPTION AND THEORETICAL ANALYSES

Figure 1 shows two schemes for the proposed laser-driven traveling-wave linac. A pair of linearly polarized laser pulses is incident on a pair of symmetric dielectric prisms, the gap between which is the channel for the electron bunch. The laser pulses initiate an evanescent guided wave in the bunch channel, which can be used for particle acceleration provided that the following Cherenkov-like conditions are satisfied [22]: the bunch velocity is greater than the speed of light in the dielectric medium, $v_e > c/n$ (where c is the speed of light in vacuum and n is the refractive index of the prism); the phase velocity of the guided wave v_p matches the particle velocity v_e (i.e., $v_p \approx v_e$); and the incident direction of the laser pulse follows the flipped Cherenkov direction, namely, the incident angle α_i shown in Fig. 1 satisfies $\alpha_i = \arcsin(c/nv_e)$. At the boundaries of the bunch channel, the laser pulses will be reflected, which then drive the next acceleration stages.

In scheme-I, a series of relay prisms are placed between cascade acceleration stages. In scheme-II, the relay prisms are removed and the laser pulses are refracted at the input and output surfaces of each prism. In both schemes, a laser pulse will experience multiple reflections and refractions through an array of microscale dielectric prisms, which can all be fabricated on a single chip, forming an effective traveling wave propagating along with the electron bunch.

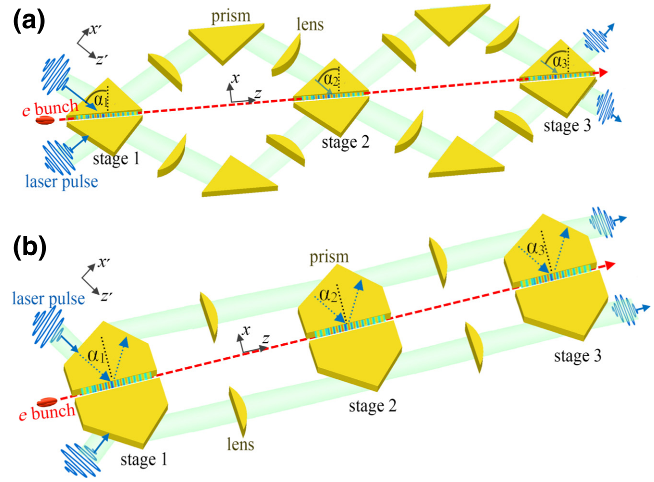

FIG. 1. Schematic diagrams of the proposed laser-driven traveling-wave linac (a) with and (b) without relay structures.

In order for the laser pulses to catch up with the electron bunch at each acceleration stage, the bunch velocity (electron energy) should satisfy specific requirements. In scheme-I, the bunch velocity should be less than the effective longitudinal velocity of the reflected light between the cascade acceleration stages and the relay stages, namely, $v_e < c \sin\alpha_i$. Using the aforementioned Cherenkov-like condition of $\sin\alpha_i = c/nv_e$, we get $v_e < c/\sqrt{n}$. Thus, the applicable bunch velocity in scheme-I should be located in the range of $c/n < v_e < c/\sqrt{n}$. In scheme-II, the laser pulses propagate parallel to the electron bunch in the longitudinal direction, so that they can certainly catch up with the electron bunch according to special relativity. Thus, any bunch velocities that satisfy the Cherenkov-like conditions can be applied in scheme-II.

The applicable electron energy as a function of the refractive index of the prism in both schemes is calculated as shown in Fig. 2. Within the applicable electron energy range, the structure parameters of the prisms and the arrangement of the multistages should be well designed according to the bunch velocity and the refractive index of the prism. In our design, we let the laser pulse catch up with the electron bunch at the midpoint of each stage [27]. The synchronization of the guided wave and accelerated particles in the cascade bunch channels can be further controlled via tuning the incident angle (α_i) of the laser pulses at each stage [24]. By these means, a single pair of short-pulse laser beams can initiate and sustain an effective traveling wave in the direction of motion of the beam, propagating along with and accelerating the particles continuously in the bunch channel, just like in a conventional rf traveling-wave linac. When the laser pulses propagate along the optical paths, diffraction is unavoidable, which may cause the laser pulses to spread, decreasing the laser

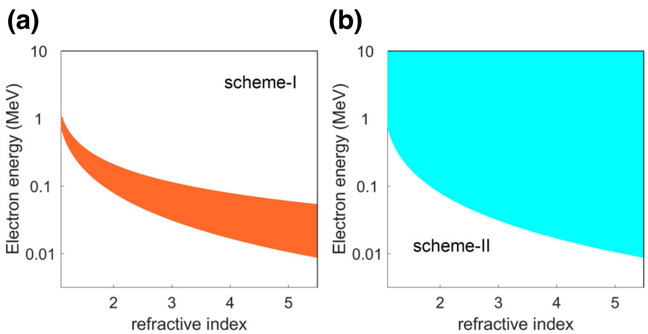

FIG. 2. The calculated applicable electron energy region (shaded) as a function of the refractive index of dielectric prisms for two schemes: (a) scheme-I and (b) scheme-II.

field intensity. To counteract diffraction, a set of focusing lenses can be used in the optical paths as shown in Fig. 2.

In practice, the incident laser pulses approximately follow Gaussian distributions, the electric field of which can be expressed as

$$E_{x'}(x', t) = E_0 e^{-(x'/w_0)^2 - 2\ln 2(t/\tau_0)^2} \cos(\omega t + \varphi_0), \quad (1)$$

in which E_0 denotes the field amplitude, x' is the transverse coordinate, w_0 is the radius of the beam waist, τ_0 is the pulse duration, ω is the angular frequency, and φ_0 is the initial phase.

We consider only the two-dimensional (2D) model, which ignores field variations in the y direction. Using Maxwell's equations and the mode-matching method in the frequency domain [28,29], the fields excited in the bunch channel of the first stage can be obtained as

$$\begin{aligned} E_x &= (k_z H_m/\omega\varepsilon_0) \sinh(k_x x)\, e^{jk_z z - [(z-z_0)\cos\alpha/w_0]^2}, \\ H_y &= H_m \sinh(k_x x)\, e^{jk_z z - [(z-z_0)\cos\alpha/w_0]^2}, \\ E_z &= (jk_x H_m/\omega\varepsilon_0) \cosh(k_x x)\, e^{jk_z z - [(z-z_0)\cos\alpha/w_0]^2}, \end{aligned} \quad (2)$$

in which ε_0 is the permittivity of vacuum, z_0 denotes the longitudinal position of the peak intensity of the Gaussian beam in the bunch channel, $k_x = \sqrt{k_z^2 - k_0^2} = \sqrt{(\omega/v_p)^2 - (\omega/c)^2}$, and

$$H_m = \frac{2\eta_1 E_0 \cos\alpha\, e^{-jk_z(\cot\alpha)g/2}}{\eta_1 \cos\alpha \sinh(k_x g/2) + j/(\omega\varepsilon_0)\, k_x \cosh(k_x g/2)}. \quad (3)$$

Here η_0 and η_1 are the wave impedances in vacuum and in the dielectric, respectively, and g is the transverse width of the bunch channel. The fields in the following stages can be obtained by using optical beam propagation methods.

With these field expressions, the particle dynamics in the bunch channel can be derived. In the longitudinal (z) direction, the particle dynamic equation reads

$$\frac{d\gamma}{dz} = \frac{2qk_x \cosh(k_x x)\,|H_m|}{m_0 c^2 \omega\varepsilon_0} e^{-[(z-z_0)\cos\alpha/w_0]^2} \sin\varphi_z, \quad (4)$$

in which q is charge quantity, $\gamma = 1/\sqrt{1-\beta^2} = 1/\sqrt{1-(v_e/c)^2}$ is the Lorentz factor, and

$$\varphi_z = \left(\frac{\omega}{v_p} - \frac{\omega}{v_e}\right) z + \varphi_0 = \delta_\varphi(z) + \varphi_0 \quad (5)$$

is the phase experienced by the particles. Here $\delta_\varphi(z)$ denotes phase slippage. In the transverse (x) direction, the particle dynamic equation reads

$$\frac{d}{dz}\left(\frac{\beta\gamma\, dx}{dz}\right) = \frac{\{2q \sinh(k_x x)\,|H_m| \cos\varphi_z\, [(1/\beta^2) - 1]\}}{m_0 c^2 \beta\varepsilon_0 v_p e^{[(z-z_0)\cos\alpha/w_0]^2}}. \quad (6)$$

III. CALCULATION AND SIMULATION

The laser propagation simulations are performed by using an electromagnetic code based on a finite-difference time-domain algorithm [30]. The parameters of the laser pulses used in the simulations and those of the designed accelerating structures, together with the initial bunch parameters, are given in Table I. Here the transverse diameter of the incident laser beam is set as 40 μm and the radius of the Gaussian beam waist w_0 is 10 μm, which had been obtained in experiments [8]. The dielectric material is chosen to be high-breakdown-threshold quartz, the refractive index (n) of which is 1.43 at wavelengths around 2 μm.

The incident angle of the laser pulse in the cascade stages (α_i) decreases gradually, which is in order to satisfy the aforementioned Cherenkov-like conditions, since the bunch velocity increases after acceleration in each stage, especially for subrelativistic electrons. In our design, α_i is chosen according to the average bunch velocity at the entrance of each stage. When the initial synchronization (as will be discussed later) is applied, it is designed so that the phase velocity of the wave in the bunch channel exactly matches the bunch velocity at the entrance of the bunch channel. In this circumstance, α_i has a specified value α_0. While, as the dynamic synchronization (as will be discussed later) is applied, α_i is designed to deviate from α_0, so that the phase velocity of the wave in the bunch channel can be greater than the bunch velocity at the entrance of the bunch channel. The deviation value is chosen to obtain the maximal energy gain for the electron bunch in the stage, as illustrated later. An ultrashort laser pulse with FWHM pulse duration of 30 fs is applied, indicating that the maximum sustainable electric field intensity of the accelerating structure (namely, the achievable acceleration gradient) can reach more than 5 GV/m [31]. In the present

TABLE I. Simulation parameters.

Symbol	Physical quantity	Value with unit
τ_0	FWHM laser pulse duration	30 fs
λ_0	Central wavelength	2 μm
w_0	Radius of the Gaussian beam waist	10 μm
w	Transverse diameter of laser beam	40 μm
E_0	Electric field amplitude	1 GV/m
n	Refractive index	1.43
$(\alpha_1, \alpha_2, \alpha_3)$	Incident angles (scheme-I)	(69.2°, 66°, 64°)
(L_1, L_2, L_3)	Channel lengths (scheme-I)	(113, 98.7, 92.7) μm
$(\alpha_1, \alpha_2, \alpha_3)$	Incident angles (scheme-II)	(54.8°, 54.3°, 53.8°)
(L_1, L_2, L_3)	Channel lengths (scheme-II)	(188, 201, 210) μm
g	Channel width	0.5 μm
E_{k1}	Initial electron energy (scheme-I)	250 keV
E_{k2}	Initial electron energy (scheme-II)	450 keV
w_t	Transverse bunch width	300 nm
σ_t	Transverse rms bunch size	50 nm
l_b	Bunch length	80 nm
σ_b	Longitudinal rms bunch size	40 nm
q	Initial bunch charge	0.1 fC
$\epsilon_{\rm nx}$	Initial transverse bunch emittance	10^{-12} m rad

paper, we choose a moderate incident field intensity of 1 GV/m.

Simulated snapshots of the laser pulse propagating in the structures at different moments are shown in Fig. 3(a). Here the results of scheme-I are illustrated [27]. We can see that the laser pulse is reflected and refracted multiple times, propagating in the cascade bunch channels at designed moments. Simulated field maps of the E_z component in the bunch channels and the distribution of the E_z field along the centerline of the bunch channel are shown in Figs. 3(b) and 3(c), respectively. Here the field distributions at the wavelength of 2 μm are illustrated. We can see that guided waves in cascade bunch channels are successfully excited. The pulse shape is largely preserved in the three cascade stages, i.e., pulse dispersion is nonsignificant. This is because each acceleration stage in the present model is so short that the waveguide dispersion in every bunch channel is negligible. In addition, the optical paths of refraction and reflection will not introduce remarkable dispersion provided that the dielectric is nondispersive. The amplitude of the laser pulse decreases gradually in the cascade stages, which is due to reflection losses at dielectric interfaces. The theoretically calculated amplitudes of the E_z field in the three channels are also shown. We can see that the calculated and simulated results agree well with each other.

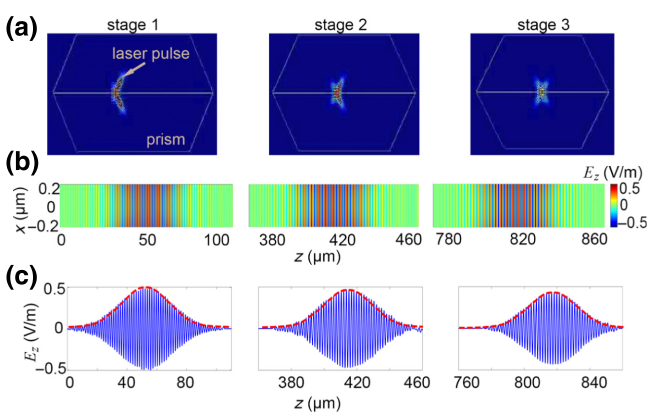

FIG. 3. (a) Simulated snapshots of the laser pulse propagating in the cascade prisms at three moments. (b) Field maps of the normalized E_z field in the bunch channels. (c) Distribution of the E_z field along the centerline of the bunch channel. The red dashed lines show the calculated profiles of the magnitude of the E_z field. Here the field intensity of the incident laser pulse is normalized to 1 V/m.

Based on the field distributions obtained above, we now consider the particle dynamics. In most previous traveling-wave accelerators, the phase velocity of the traveling (guided) wave was set to match the initial bunch velocity at the entrance of an accelerating structure (hereinafter referred to as initial synchronization). Using the particle dynamic equations, the phase experienced by particles under the initial synchronization condition, together with the electron energy, is calculated in Fig. 4(a) (shown by dotted lines). Here the results of a single particle at the transverse position of $x = 10$ nm in the first acceleration stage of scheme-I are shown. We can see that the phase experienced by the particle increases monotonically (slips) from $-3\pi/4$ (acceleration region) to $3\pi/4$ (deceleration region). The electron energy first increases and then decreases, so that the effective acceleration length and energy gain are restricted.

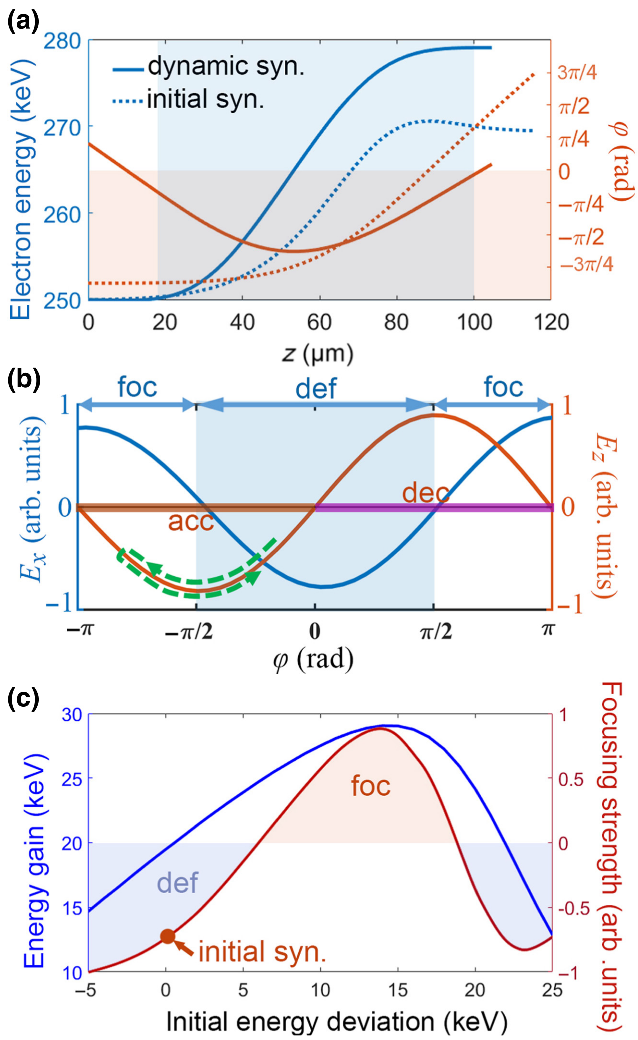

FIG. 4. (a) Calculated phase and electron energy of a particle as functions of longitudinal position. Here the initial synchronous phases of the particles in both the initial and dynamic synchronization cases are optimized to get relatively maximum energy gains (hereinafter inclusive). The horizontal shaded region denotes the acceleration phases and the longitudinal one denotes the region of laser-excited fields in the channel. (b) Simulated E_x and E_z fields versus phase observed at the position of $x = 10$ nm in the bunch channel. The green dashed arrowed line denotes the phase slipping for the dynamic synchronization method. (c) Optimized energy gain and corresponding transverse focusing strength versus the deviation of initial electron energy.

In order to counteract dephasing and to increase energy gain, here we propose a dynamic synchronization method, in which the phase velocity of the guided wave in the bunch channel is set to be greater than the initial particle velocity and to be less than the final particle velocity after acceleration in each stage. Thus, the phase experienced by the particle will first slip toward and then away from an effective synchronization phase. Applying the dynamic synchronization method, the phase experienced by the particle, together with its energy gain, is also calculated in Fig. 4(a) (shown by solid lines). Here the corresponding electron energy of the phase velocity is 15 keV greater than the initial electron energy. We can see that the phase experienced by the particle first decreases and then increases as predicted. Compared with that of the initial synchronization case, the net phase slippage is greatly reduced. The particle is almost entirely located in the acceleration region in the whole bunch channel of an accelerating stage, so that the energy gain is obviously enhanced.

Next, we discuss bunch spread and deflection, which are caused by space-charge and emittance effects, as well as by the transverse electromagnetic fields in the bunch channel. We will show that bunch spread and deflection can also be greatly mitigated by using the dynamic synchronization method. As indicated by Eq. (2), the longitudinal field (E_z) and the transverse fields (E_x and H_y) in the bunch channel have $\pi/2$ phase differences, which is verified by the simulations shown in Fig. 4(b). In addition, the longitudinal and transverse focusing are in opposite regions, so that transverse focusing will lead to longitudinal spread. In the dynamic synchronization case, the synchronous phase will first slip from transverse defocusing (longitudinal compression) region to focusing (longitudinal spread) region and then return back, as illustrated by the green dashed arrowed line in Fig. 4(b). Thus, an electron bunch will experience a transverse defocusing-focusing-defocusing (longitudinal compression-decompression-compression) process in each acceleration stage, by which the dynamic focusing of the electron bunch can be realized, similarly as in the alternating-phase focusing method for an inverse Smith-Purcell accelerator [32–34].

In practice, considering the space-charge and emittance effects, in order to enhance the pass ratio of particles in a tiny-size bunch channel, the net force of the transverse electromagnetic fields exerted on the electron bunch should be a convergent force. The overall transverse focusing strength can be evaluated by integrating the transverse dynamic equation (6) along the bunch channel. Figure 4(c) shows the optimized energy gain and transverse focusing strength of particles in the dynamic synchronization case, in which the corresponding electron energy of the phase velocity deviates from the initial electron energy of particles (zero deviation denotes initial synchronization case). Here the positive and negative values of the transverse focusing strength denote focusing and defocusing effects, respectively. We can see that, for the initial synchronization case, the transverse focusing strength is negative, indicating that the transverse fields exert a net defocusing effect on the electron bunch, which will spread quickly in the process of acceleration. For the dynamic synchronization case, the transverse focusing strength can be a positive value, reaching a maximum as the initial electron energy deviation is about 14 keV. Under this circumstance, both high energy gain and beam focusing can be realized. For a multistage cascade accelerator in practice, the phase velocities of guided waves in each stage can be optimized (via changing the prism angles) to acquire a maximum total energy gain [27].

In order to verify the theoretical analyses, the bunch dynamics are simulated by using the General Particle Tracer (GPT) code [35]. In simulations, each electron bunch initially consists of 500 macroparticles, which follow truncated Gaussian distributions in both the z and x directions. In order to simulate the 2D model, the particles in the bunch are set to be uniformly distributed along a 20-μm range in the y direction. The bunch width in the x direction is set to be 300 nm and the root-mean-square (rms) bunch size is 50 nm. The total bunch length is 80 nm and the rms bunch length is 40 nm. The corresponding durations of the electron bunches in scheme-I and scheme-II are 0.36 fs and 0.32 fs, respectively. Namely, the duration of the electron bunch used in the simulation is much less than a half-cycle of the laser wave, so that the whole bunch can be accelerated, as will be shown. We note that similar ultrashort electron bunches have already been realized in experiment [36]. Other bunch parameters are given in Table I.

The space-charge and emittance effects are taken into consideration. The simulated transverse phase-space x-β_x distributions (β_x is the ratio of the particle velocity in the x direction to the speed of light in vacuum) of particles in the bunch observed, respectively, at the front, middle, and rear parts in each acceleration stage of scheme-I are shown in Fig. 5, in which the results of the initial synchronization case are also shown (in red) for comparison. We can see that, for the initial synchronization case, almost all of the particles are in the defocusing phase state in the whole bunch channel, so that the electron bunch will spread quickly in the process of acceleration, restricting the pass ratio, as will be shown. While, for the dynamic synchronization case, the electron bunch is in the defocusing state in the front part of the bunch channel and is then largely transformed to the focusing state in the middle part of the bunch channel. At the rear part, although some particles return to the defocusing state, most of the particles are in the focusing phase state, and the main part of the electron bunch is focused in the bunch channel. In other words, the electron bunch will first spread and then be focused by the transverse electromagnetic forces in the bunch channel, agreeing with theoretical predictions. This process is almost repeated in each acceleration stage.

We note that the phase space of the electron bunch increases in the bunch channel, which can be explained as follows. Since the electron bunch has definite size and charge distribution, the particles at different positions in the bunch will experience different phases of electromagnetic fields, namely different longitudinal (acceleration) and transverse (deflection) forces, which will increase the total emittance of the bunch. Figure 6 shows the simulated pass ratio of the electron bunch in the cascade acceleration channels of both scheme-I and scheme-II. Here the particles that are physically located outside the bunch channel in each acceleration stage have been removed. The sharp decreases at the entrances of the second and third stages are due to the bunch spread as drifting between two cascade stages. We can see that, compared with that in the initial synchronization case, the pass ratio of the electron bunch in the dynamic synchronization case is greatly enhanced. For scheme-I, the final pass ratio through three stages is increased from 2% to 43%, and for scheme-II, it is increased from 7% to 68%. We envisage that the pass ratio can be further increased via using the recently proposed laser-driven electron lensing method [37] to focus the electron bunch in the drifting regions between adjacent acceleration stages.

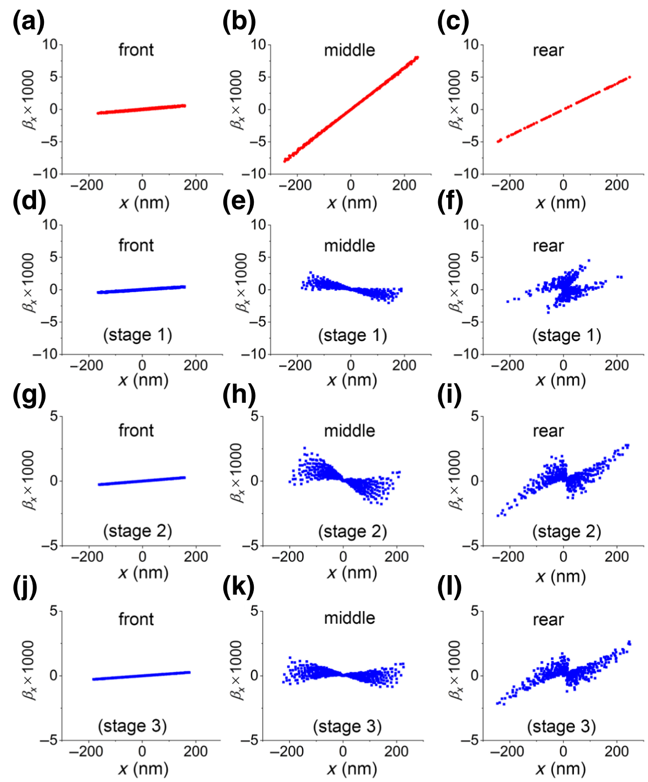

FIG. 5. Simulated phase-space (x-β_x) distributions of the particles in the bunch, respectively at the front, middle, and rear parts in each acceleration stage of scheme-I. (a)–(c) The results of the initial synchronization case. (d)–(l) The results for the dynamic synchronization case in (d)–(f) stage 1, (g)–(i) stage 2, and (j)–(l) stage 3.

Figures 7(a) and 7(b) show the calculated and simulated electron energy versus propagation distance in both schemes. In the theoretical results, the energy of a single particle is calculated, and in the simulated results, the average electron energy of the whole bunch is presented,

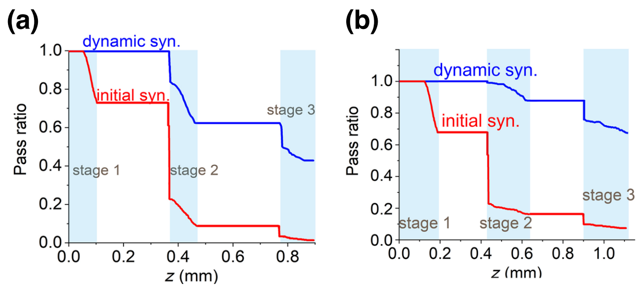

FIG. 6. Simulated pass ratio versus propagation distance for (a) scheme-I and (b) scheme-II.

which is why the simulated electron energy is less than the calculated one. We can see that the whole electron bunch is continually accelerated in the cascade acceleration stages, as predicted. The energy gain reaches 50–60 keV after three cascade acceleration stages with total length of $\sim$ 1 mm.

Figures 7(c) and 7(d) further show the simulated energy spectra of the electron bunch after each acceleration stage. We note that the FWHM energy spread of the bunch first increases (see stage 1 and stage 2) and then decreases (see stage 3) in the process of acceleration. This is because the particles with a large energy deviation have been removed by the boundaries of the bunch channels. In other words, the surviving particles will be largely focused into a small phase space after cascade acceleration stages.

Figure 8 shows the simulated transverse emittance of the electron bunch versus propagation distance in both schemes. We note that the bunch emittance grows obviously, especially in the second and third stages, which is

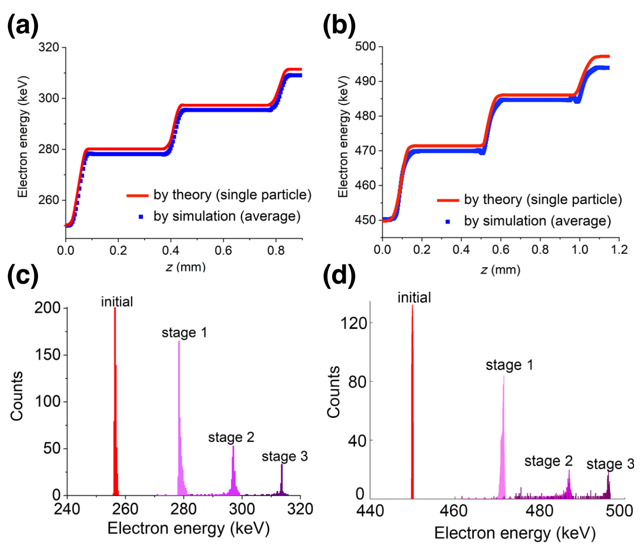

FIG. 7. Calculated and simulated electron energy versus propagation distance for (a) scheme-I and (b) scheme-II. Simulated energy spectra of the electron bunch after three cascade acceleration stages for (c) scheme-I and (d) scheme-II.

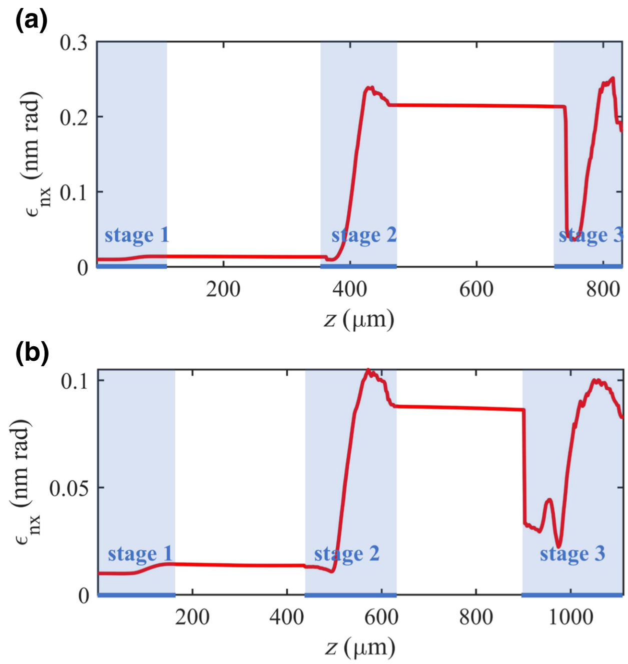

FIG. 8. Simulated x-direction emittance of the electron bunch versus propagation distance for (a) scheme-I and (b) scheme-II.

because different parts of the bunch experience different forces as they traverse the bunch channel. Also, we note that, at the entrances and the rear portions of the second and third stages, the bunch emittance decreases noticeably, which is because the particles located at the fringe of the bunch have been removed by the boundaries of the bunch channel. Hence, the final bunch emittance after cascade acceleration is limited, which is less than 0.3 nm rad in scheme-I and less than 0.1 nm rad in scheme-II.

IV. DISCUSSIONS AND CONCLUSION

In this section, we discuss several critical factors that affect the practical implementation of the proposed schemes. We first look at the energy gain of the accelerated particles, which is restricted to be at the level of tens of kiloelectronvolts after three cascade accelerations, as presented. The main restriction of energy gain in the proposed schemes is the phase slippage in each acceleration stage. As shown in Fig. 4(a), the effective acceleration length in each stage is about 60 μm due to phase slippage, so that the energy gain in each stage is restricted to tens of kiloelectronvolts even though the actual acceleration gradient reaches 500 MV/m. In fact, this is also the main obstacle for almost all of the available dielectric laser accelerators.

In order to alleviate the phase slippage and to increase energy gain, two methods could be applied. Firstly, laser beams with longer wavelengths could be used to drive the acceleration structures. According to Eq. (5), the phase slippage is proportional to the frequency of the laser beam;

in other words, the effective acceleration length is proportional to the wavelength of the drive laser. Thus, if we use a CO_2 laser with wavelength of about 10 μm, both the acceleration length and the energy gain will be increased by a factor of 5. Secondly, in order to further increase the acceleration length and energy gain, prisms with curved input and output surfaces, which are similar to convex lenses, can be applied. In prisms with curved surfaces, the incident direction of the laser pulse changes gradually in the process of bunch acceleration, which is similar to what happens in a prism with crevices, as presented in Ref. [24]. Thus the Cherenkov synchronization condition can be continually satisfied for a velocity-changing particle, i.e., the phase slippage is counteracted. Our further research shows that, by using prisms with well-designed curved surfaces, the acceleration length and energy gain can be further increased by several times. It is predicted that, by using these two methods, a megaelectronvolt-level electron beam can be realized from a chip-based acceleration structure.

Next, we discuss the effect of fabrication precision of dielectric structures on the performance of the proposed schemes. According to the analyses and simulations, the structure parameters are essential for the field distributions in the bunch channels, which determine the fields and phases experienced by the electron bunch. However, when the dynamic synchronization method proposed in the present paper is applied, the phase and amplitude of the fields experienced by the electron bunch are dynamic values within a certain range rather than definite steady ones, so that the requirements of exact phase and amplitude values are avoided. In addition, the phase and amplitude can be readily adjusted by changing the initial electron energy and the time delay of the laser pulse in practice. Hence, the dynamic synchronization method is helpful to alleviate the requirement of nanoscale fabrication precision of acceleration structures.

In conclusion, we have proposed a novel concept of a laser-driven traveling-wave linac on a chip, together with a dynamic synchronization and focusing method, which can simultaneously realize the nondispersive propagation of laser pulses along acceleration structures, stable bunch transport in a tiny-size bunch channel, and continuous synchronization of subrelativistic particles with laser-driven fields, achieving the full-course acceleration and focusing of particles by using a single laser source, without resorting to external focusing equipment. This is crucial for miniaturization of a particle accelerator, paving the way toward a high-efficiency on-chip particle accelerator for practical applications.

ACKNOWLEDGMENTS

This work is supported by the Natural Science Foundation of China (Grants No. U1632150, No. 12075239, and No. 61471332) and by the Fundamental Research Funds for the Central Universities (Grant No. NS2022042).

[1] R. J. England, *et al.*, Dielectric laser accelerator, Rev. Mod. Phys. **86**, 1337 (2014).

[2] B. Neuner III, D. Korobkin, G. Ferro, and G. Shvets, Prism-coupled surface wave accelerator based on silicon carbide, Phys. Rev. Spec. Top. Accel. Beams **15**, 031302 (2012).

[3] E. A. Peralta, K. Soong, R. J. England, E. R. Colby, Z. Wu, B. Montazeri, C. McGuinness, J. McNeur, K. J. Leedle, D. Walz, E. B. Sozer, B. Cowan, B. Schwartz, G. Travish, and R. L. Byer, Demonstration of electron acceleration in a laser-driven dielectric microstructure, Nature **503**, 91 (2013).

[4] J. Breuer and P. Hommelhoff, Laser-Based Acceleration of Nonrelativistic Electrons at a Dielectric Structure, Phys. Rev. Lett. **111**, 134803 (2013).

[5] Adi Hanuka and Levi Schachter, Bragg accelerator optimization, High Power Laser Sci. Eng. **2**, e24 (2014).

[6] U. Niedermayer, J. Lautenschlager, T. Egenolf, and O. Boine-Frankenheim, Design of a Scalable Integrated Nanophotonic Electron Accelerator on a Chip, Phys. Rev. Appl. **16**, 024022 (2021).

[7] A. Hanuka and L. Schachter, Operation of dielectric laser accelerators: Single bunch, Phys. Rev. Accel. Beams **21**, 054001 (2018).

[8] K. J. Leedle, R. F. Pease, R. L. Byer, and J. S. Harris, Laser acceleration and deflection of 96.3 keV electrons with a silicon dielectric structure, Optica **2**, 158 (2015).

[9] K. P. Wootton, Z. Wu, B. M. Cowan, A. Hanuka, I. V. Makasyuk, E. A. Peralta, K. Soong, R. L. Byer, and J. R. England, Demonstration of acceleration of relativistic electrons at a dielectric microstructure using femtosecond laser pulses, Opt. Lett. **41**, 2696 (2016).

[10] J. Breuer and P. Hommelhoff, Dielectric laser acceleration of 28 keV electrons with the inverse Smith-Purcell effect, Nucl. Instrum. Methods Phys. Res. A **740**, 114 (2014).

[11] J. Breuer, R. Graf, A. Apolonski, P. Hommelhoff, and Dielectric laser acceleration of nonrelativistic electrons at a single fused silica grating structure: Experimental part, Phys. Rev. Spec. Top. Accel. Beams **17**, 021301 (2014).

[12] R. J. England, A. Kwiatkowski, C.-K. Ng, and Z. Wu, Input coupling for photonic bandgap fiber accelerators, IEEE J. Sel. Top. Quantum Electron. **22**, 4401109 (2016).

[13] A. Mizrahi and L. Schachter, Optical Bragg accelerators, Phys. Rev. E **70**, 016505 (2004).

[14] X. E. Lin, Photonic band gap fiber accelerator, Phys. Rev. Spec. Top. Accel. Beams **4**, 051301 (2001).

[15] B. M. Cowan, Three-dimensional dielectric photonic crystal structures for laser-driven acceleration, Phys. Rev. Spec. Top. Accel. Beams **11**, 011301 (2008).

[16] P. P. Pronko, P. A. VanRompay, C. Horvath, F. Loesel, T. Juhasz, X. Liu, and G. Mourou, Avalanche ionization and dielectric breakdown in silicon with ultrafast laser pulses, Phys. Rev. B **58**, 2387 (1998).

[17] N. V. Sapra, K. Y. Yang, D. Vercruysse, K. J. Leedle, D. S. Black, R. J. England, L. Su, R. Trivedi, Y. Miao, O. Solgaard, R. L. Byer, and Jelena Vuckovic, On-chip integrated laser-driven particle accelerator, Science **367**, 79 (2020).

[18] Tyler W. Hughes, R. Joel England, and Shanhui Fan, Reconfigurable Photonic Circuit for Controlled Power Delivery to Laser-Driven Accelerators on a Chip, Phys. Rev. Appl. **11**, 064014 (2019).

[19] S. Tan, Z. Zhao, K. Urbanek, T. Hughes, Y. Jo Lee, S. Fan, J. S. Harris, and R. L. Byer, Silicon nitride waveguide as a power delivery component for on-chip dielectric laser accelerators, Opt. Lett. **44**, 335 (2019).

[20] A. Lohmann, Electron acceleration by light waves, IBM Tech. Note **5**, 169 (1962).

[21] M. Kozak, P. Beck, H. Deng, J. Mcneur, N. Schonenberger, C. Gaida, F. Stutzki, M. Gebhardt, J. Limpert, A. Ruehl, I. Hartl, O. Solgaard, J. S. Harris, R. L. Byer, and P. Hommelhoff, Acceleration of sub-relativistic electrons with an evanescent optical wave at a planar interface, Opt. Express **25**, 19195 (2017).

[22] W. Liu, Z. Yu, L. Sun, Y. Liu, Q. Jia, H. Xu, and B. Sun, Microscale Laser-Driven Particle Accelerator Using the Inverse Cherenkov Effect, Phys. Rev. Appl. **14**, 014018 (2020).

[23] B. R. Frandsen, S. A. Glasgow, and J. B. Peatross, Acceleration of free electrons in a symmetric evanescent wave, Laser Phys. **16**, 1311 (2006).

[24] W. Liu, L. Sun, Z. Yu, Y. Liu, Q. Jia, B. Sun, and H. Xu, THz-driven dielectric particle accelerator on chip, Opt. Lett. **46**, 4398 (2021).

[25] L. Sun, W. Liu, J. Zhou, Y. Zhu, Z. Yu, Y. Liu, Q. Jia, B. Sun, and H. Xu, GV m^{-1} on-chip particle accelerator driven by few-cycle femtosecond laser pulse, New J. Phys. **23**, 063031 (2021).

[26] L. Zhang, W. Liu, Y. Liu, Q. Jia, B. Sun, H. Xu, S. Liu, Inverse Cherenkov dielectric laser accelerator for ultra-relativistic particles, J. Phys. D Appl. Phys. **56**, 045103 (2023).

[27] See Supplemental Material at http://link.aps.org/supplemental/10.1103/PhysRevApplied.19.044066 for the detailed derivation process in obtaining the structure parameters, for the simulated laser propagation results in scheme-II together with the cartoons of laser pulse propagation in both schemes, and for the calculated results of energy gains and transverse focusing strengths in the cascade stages of both schemes.

[28] H. Raether, *Plasmons on Smooth and Rough Surfaces and on Gratings* (Springer-Verlag, Berlin, 1988).

[29] K. Zhang and D. Li, *Electromagnetic Theory in Microwave and Optoelectronics* (Springer-Velag, Berlin, 2008).

[30] CST Corp., CST PS Tutorials. https://www.3ds.com/products-services/simulia/products/cst-studio-suite/.

[31] D. Cesar, S. Custodio, J. Maxson, P. Musumeci, X. Shen, E. Threlkeld, R. J. England, A. Hanuka, I. V. Makasyuk, E. A. Peralta, K. P. Wootton, and Z. Wu, High-field nonlinear optical response and phase control in a dielectric laser accelerator, Commun. Phys. **1**, 46 (2018).

[32] R. Shiloh, J. Illmer, T. Chlouba, P. Yousefi, N. Schönenberger, U. Niedermayer, A. Mittelbach, P. Hommelhoff, Electron phase-space control in photonic chip-based particle acceleration, Nature **597**, 498 (2021).

[33] U. Niedermayer, T. Egenolf, and O. Boine-Frankenheim, Three Dimensional Alternating-Phase Focusing for Dielectric-Laser Electron Accelerators, Phys. Rev. Lett. **125**, 164801 (2020).

[34] U. Niedermayer, T. Egenolf, O. Boine-Frankenheim, and P. Hommelhoff, Alternating-Phase Focusing for Dielectric Laser Acceleration, Phys. Rev. Lett. **121**, 214801 (2018).

[35] General Particle Tracer (GPT), Pulsar Physics. http://www.pulsar.nl/.

[36] N. Schonenberger, A. Mittelbach, P. Yousefi, J. McNeur, U. Niedermayer, and P. Hommelhoff, Generation and Characterization of Attosecond Microbunched Electron Pulse Trains via Dielectric Laser Acceleration, Phys. Rev. Lett. **123**, 264803 (2019).

[37] Dylan S. Black, Kenneth J. Leedle, Yu Miao, Uwe Niedermayer, Robert L. Byer, and Olav Solgaard, Laser-Driven Electron Lensing in Silicon Microstructures, Phys. Rev. Lett. **122**, 104801 (2019).